

# Dense, thin clouds and reprocessed radiation in the central regions of Active Galactic Nuclei

Z. Kuncic<sup>1</sup>\*, A. Celotti<sup>1,2</sup> and M. J. Rees<sup>1</sup>

<sup>1</sup>*Institute of Astronomy, Madingley Rd, Cambridge CB3 0HA*

<sup>2</sup>*SISSA/ISAS, via Beirut 4, 34014 Trieste, Italy*

## ABSTRACT

The primary radiation generated in the central continuum-forming region of Active Galactic Nuclei (AGN) can be reprocessed by very dense, small-scale clouds that are optically-thin to Thomson scattering. In spite of the extreme conditions expected to prevail in this innermost, central environment, the radiative clouds can survive and maintain cool temperatures relative to the ambient emitting region by means of confinement by strong magnetic fields. Motivated by these ideas, we present a detailed quantitative study of such clouds, explicitly describing the physical properties they can attain under thermal and radiative equilibrium conditions. We also discuss the thermal stability of the gas in comparison to that of other reprocessing material thought to reside at larger distances from the central source. We construct a model to predict the emergent spectra from a source region containing a total line of sight column density  $\lesssim 10^{23} \text{ cm}^{-2}$  of dense clouds which absorb and reemit the primary radiation generated therein. Our predicted spectra show the following two important results: (i) the reprocessed flux emitted at optical/UV energies is insufficient to account for the blue bump component in the observed spectra; and (ii) the amount of line radiation that is emitted is at least comparable to (and in many cases dominates) the continuum radiation. The lines are extremely broad and tend to accumulate in the extreme ultraviolet (EUV), where they form a peak much more prominent than that which is observed in the optical/UV. This result is supported by current observations, which indicate that the spectral energy distribution (SED) of radio-quiet AGN may indeed reach a maximum in the EUV band.

**Key words:** galaxies: active — atomic processes, radiative transfer

## 1 INTRODUCTION

There is mounting observational evidence that the centres of most AGN harbour vast quantities of thermal matter and that this material plays a key role in the generation of the observed spectra by reprocessing the primary radiation. The importance of reprocessing by relatively cool ( $\sim 10^5$  K), dense gas in the central environments of AGN is clearly evident from the observed X-ray spectra, particularly those of Seyfert nuclei, which typically exhibit a variety of distinct thermal signatures in the form of lines, edges and reflection features (e.g. Pounds et al. 1990; Nandra et al. 1991; Nandra & Pounds 1994). However, the most compelling evidence for the presence of energetically-significant amounts of cool material in the central regions of radio-quiet quasars and Seyferts (which comprise the vast majority of AGN) is

provided by the excess of optical/UV over X-ray continuum radiation known as the ‘blue bump’ (Shields 1978; Edelson & Malkan 1986; Elvis et al. 1994). This is typically the most prominent component in the SED of these objects and can contain as much as half of the entire observed spectral power (e.g. Neugebauer et al. 1987; Sanders et al. 1989; Kolman et al. 1993). The soft X-ray excess that is often seen above an extrapolation of the X-ray power law (Arnaud et al. 1985; Wilkes & Elvis 1987; Walter & Fink 1993) may be the high energy tail of the blue bump and indeed, recent observations imply a link between the two components, with the possibility that they constitute a single ‘big bump’ component extending from the optical/UV band up to soft X-rays (see Puchnarewicz et al. 1996 and references cited therein).

In the framework of the standard black hole paradigm for AGN (Rees 1984), any optically-thick thermal gas residing within about 100 gravitational radii, regardless of its distribution, is expected to produce a quasi-blackbody spectrum that peaks at  $\sim 10^5$  K. Since the bulk of the accreting material is expected to fall into an optically-thick

\* Present address: ANU Astrophysical Theory Centre, School of Mathematical Sciences, Australian National University, ACT 0200, Australia, E-mail: kuncic@maths.anu.edu.au

disk, this is the most natural explanation for the blue bump (Shields 1978; Malkan & Sargent 1982; Czerny & Elvis 1987; Sun & Malkan 1989). Although the thermal character of the blue bump is now independently confirmed (Koratkar et al. 1995), detections of quasi-simultaneous optical and UV variations (e.g. Courvoisier & Clavel 1991; Clavel et al. 1992) are inconsistent with the radiation being ‘intrinsic’ to a standard accretion disk (i.e. emitted as a result of internal dissipation). These variability measurements suggest instead that the blue bump is probably ‘secondary’ radiation that has been reprocessed by the disk (e.g. Lightman & White 1988; George & Fabian 1991). Indeed, the presence of relatively cool reprocessing material in a disk within 20 gravitational radii of a central mass is inferred from the very recent ASCA X-ray observations (Tanaka et al. 1995).

However, not all cool gas at the centres of AGN need necessarily reside in the putative accretion disk. Some may be distributed in the form of numerous dense clouds or filaments which occupy only a small fraction of the total volume of the source region but which provide a substantial covering factor (Guilbert & Rees 1988). Indeed, several models which calculate the reprocessed spectra due to optically-thick clouds are successful in reproducing the general features of the observed X-ray spectra (e.g. Sivron & Tsuruta 1993; Bond & Matsuoka 1993; Nandra & George 1994). However, the absence of a strong soft X-ray cutoff in the observed spectra of some objects limits the line of sight column densities to  $\lesssim 10^{21} \text{ cm}^{-2}$  (e.g. Turner & Pounds 1989) or to slightly higher values ( $\sim 10^{23} \text{ cm}^{-2}$ ) if the gas is warmer and hence, more highly-ionized (Nandra et al. 1991). This means that clouds with a significant Thomson optical depth residing within the primary source region where the X-rays are produced must have a covering factor less than unity so that not all the X-rays are intercepted, as implied by the soft X-ray absorption limits.

Clouds can be distributed throughout the central source region with a large covering factor (close to unity) if they are optically-thin to Thomson scattering. These clouds might contribute to the optical/UV blue bump (Celotti, Fabian, & Rees 1992, hereafter CFR92) and indeed, some models even attribute the blue bump to such reprocessing material (Barvainis 1993). The presence of Thomson-thin reprocessing gas could also be postulated from the observed spectra of quasars, which typically lack a reflection component, but which exhibit a blue bump that is energetically more significant than the X-ray flux (Williams et al. 1992; Elvis et al. 1994). However, Thomson-thin clouds must be extremely dense in order to keep cool and to produce distinct thermal signatures in the observed spectra. As examined by Ferland & Rees (1988; hereafter FR88), the radiative equilibrium of very dense gas irradiated by an intense AGN source is dominated by free-free absorption. Induced processes can also be important, as well as photoionization and recombination, which are the dominant processes for the cooler gas in the more distant broad line region (BLR) in AGN (see e.g. Osterbrock 1985).

In the central continuum-forming region of AGN, a plausible scenario is that dense clouds are embedded within a hot, magnetically-dominated gas which pervades the source region, forming a corona above and below the inner disk (e.g. Svensson & Zdziarski 1995; Zdziarski & Magdziarz 1996). The strong magnetic fields which could be responsible

for accelerating the radiating particles can also provide the chief means of cloud confinement required in such a multi-phase medium (Rees 1987). Moreover, the confining magnetic stresses can, by suppressing transverse conductivity, effectively insulate the clouds from the external hot plasma and, in the presence of strong radiation forces, can maintain the very small scalesizes that are implied by the high densities and the column density constraint inferred from the lack of strong soft X-ray extinction. In this case ‘clouds’ may ultimately manifest themselves as magnetospheric filaments or streaks, depending on the field configuration (CFR92; see also Kuncic, Blackman, & Rees 1996).

Indeed, the presence of dense clouds in sources where the magnetic and radiation fields are in equipartition can explain the lack of correlated variability between IR/optical and X-ray fluxes (detected in at least one object – see Celotti, Ghisellini, & Fabian 1991), since free-free absorption is capable of depleting all of the low frequency radiation from a primary source. When the free-free absorption extends up to optical/UV frequencies ( $\sim 10^{15} \text{ Hz}$ ), it is energetically possible that reprocessing by free-free absorbing clouds can ultimately produce a significant fraction of the blue bump, as suggested by CFR92.

At temperatures  $\sim 10^5 \text{ K}$ , the radiation reemitted from such gas is expected to comprise free-free (bremsstrahlung) and bound-free emission due to hydrogen and, to a lesser extent, helium nuclei, as well as line emission (bound-bound transitions) due to heavier nuclei. In practice, it is necessary to consider the thermal and ionization balance of the reprocessing gas as well as radiative transfer effects in order to determine the relative importance of these processes and to predict the emergent spectra from a collection of clouds.

In this paper, we use a numerical code to obtain explicitly the physical properties (temperature and ionization structure) acquired by very dense clouds in thermal and radiative equilibrium and to calculate the emergent spectra from a source region containing such clouds. Our objective is to further study and extend the ideas presented by CFR92 by determining whether cool temperatures and small column densities are compatible radiative equilibrium properties of dense clouds which might reside in an AGN magnetosphere. We reexamine an earlier attempt by FR88 at predicting the spectra from similar clouds by constructing a more self-consistent model which explicitly takes into account line emission and the reprocessed radiation field. We also compare in closer detail the predicted spectra with current observations. In Section 2, we state the specifications and assumptions of our numerical analysis, while in Sections 3 and 4, respectively, we study the thermal structure and stability of isolated dense clouds. In Section 5, the emergent spectra predicted by our cloud model are presented and compared with the observed SEDs of radio-quiet AGN. We summarize our results and their implications in Section 6.

## 2 ASSUMPTIONS AND SPECIFICATIONS

### 2.1 Radiative Equilibrium

Dense clouds residing at the centres of AGN can attain radiative equilibrium and thereby contribute to the observed spectrum by absorbing and reemitting the primary radiation

provided that they can survive for at least a few radiative lifetimes,  $t_{\text{rad}}$ . This is the case for a wide range of reasonable parameters. The clouds must be small enough to come into pressure equilibrium with their surroundings, which requires the sound-crossing time to be shorter than the characteristic dynamical timescale,  $t_{\text{dyn}}$ . On the other hand, the clouds cannot be so small that they are too quickly destroyed by microphysical diffusion processes (Kuncic, Blackman, & Rees 1996). For the clouds to sustain cool temperatures, there is also the requirement that  $t_{\text{rad}}$  must be shorter than  $t_{\text{dyn}}$ . The longest radiative cooling timescale for partially-ionized gas with an electron temperature  $T_e$  and number density  $n_e$  is typically that for bremsstrahlung emission due to electron encounters with ions,

$$t_{\text{rad}} \sim 10^{13} n_e^{-1} \left( \frac{T_e}{10^5 \text{ K}} \right)^{1/2} \text{ s.}$$

An indication on  $t_{\text{dyn}}$  in the primary source region comes from the observed timescale for X-ray variability. This is typically on the order of hours, although variability timescales as short as 100 s have been measured in some objects (see Mushotzky, Done, & Pounds 1993 for a review). Thus, over these timescales, thermal gas with electron densities  $n_e \gg 10^{11} \text{ cm}^{-3}$  can maintain radiative equilibrium in the central regions of AGN.

Since the absorption and emission rates of the specific radiation processes have a complex temperature dependence and the total heating and cooling rates further depend on the coupling between the local temperature and ambient radiation field, as described by the radiative transfer equation, a self-consistent thermal and radiative equilibrium solution  $T_e$  can only be evaluated with the use of statistical equations and numerical iterative methods. We employ the code CLOUDY (version 84.09) (Ferland 1993), which calculates the radiative equilibrium properties of thermal gas that is optically-thin to Thomson scattering. This code has been previously tested by FR88 for its application to the case of an intense nonthermal AGN source irradiating clouds with a range of densities. The code calculates a self-consistent equilibrium electron temperature  $T_e$  at discrete points within a cloud of given density and size, for certain specifications and assumptions about the total flux and spectral shape of the incident radiation, the chemical composition of the gas and the cloud geometry. These are described next.

## 2.2 The Primary Radiation Field

The high-energy spectra of radio-quiet quasars and Seyferts are understood to comprise a reprocessed component that is flatter in the 2-30 keV range (e.g. Pounds et al. 1990; Nandra & Pounds 1994). Taking this into account, we assume a primary radiation field composed of a power-law component which extends over X-ray energies with a spectral index  $\alpha \equiv -d \log F_\nu / d \log \nu = 1.0$  that is consistent with the observed spectra when the reprocessing features are decoupled. We assume that this primary spectrum steepens to an index of 2.0 above a break energy in hard X-rays at 100 keV, as predicted by the currently-favoured thermal Comptonization models (e.g. (Haardt & Maraschi 1993; Stern et al. 1995)). Although there is some evidence from typical Seyfert 1 spectra for such a high-energy cutoff, it is not very well constrained by the observations (e.g. Maisack et al. 1993; John-

son 1994; Zdziarski et al. 1995). However, the uncertainty in its precise location will not affect the radiative equilibrium of the dense gas we investigate here, since with the low column densities we consider, the gas is only weakly coupled to such hard radiation. At low frequencies, we assume a self-absorbed synchrotron spectrum with a FIR turnover frequency  $\nu_t$  (see de Kool & Begelman 1995).

Specifically, we describe this primary radiation with a mean intensity (erg.s<sup>-1</sup>cm<sup>-2</sup>Hz<sup>-1</sup>)

$$j_\nu \propto \begin{cases} \nu^{5/2} & , \quad h\nu \lesssim h\nu_t \\ \nu^{-1} & , \quad h\nu_t \lesssim h\nu \lesssim 100 \text{ keV} \\ \nu^{-2} & , \quad h\nu \gtrsim 100 \text{ keV.} \end{cases}$$

In the present context, it is instructive to normalize this primary spectrum with a total flux expressed in terms of a radiation energy-density temperature  $T_{\text{rad}}$ , since this is just the equivalent blackbody temperature which is attained in the optically-thick limit, defined by (see FR88)

$$aT_{\text{rad}}^4 = \frac{4\pi}{c} \int d\nu j_\nu = \frac{L}{4\pi r^2 c},$$

where  $L$  is the total bolometric luminosity,  $r$  is the size of the source region and  $a$  is the usual radiation energy-density constant. To explore the properties of clouds in high and low radiation energy-density environments, we use the limits of the range  $5 \times 10^4 \text{ K} \lesssim T_{\text{rad}} \lesssim 2 \times 10^5 \text{ K}$ . The upper and lower bounds of this range would correspond to a source of size  $r \sim 10r_g$  and  $r \sim 100r_g$ , respectively, radiating at the Eddington limit of a black hole of mass  $10^7 M_\odot$ , with a gravitational radius  $r_g \sim 1.5 \times 10^{12} \text{ cm}$ .

Because of the high intensity of the primary radiation field in the central continuum-forming region, it is of interest to examine the effects of different maximum brightness temperatures,  $T_\nu \equiv (c^2/2k\nu^2)j_\nu$ , and to do so, we choose two extreme values of the self-absorption turnover frequency:  $\nu_t = 3 \times 10^{13} \text{ Hz}$  and  $\nu_t = 5 \times 10^{14} \text{ Hz}$ . The value of  $\nu_t$  affects gas heating, not only via free-free absorption, but also via Compton scattering, which can be enhanced by the extra contribution of induced scattering. Induced Compton scattering has an optical depth which differs from the Thomson optical depth  $\tau_T$  by a factor  $kT_\nu/m_e c^2$ ; it can be important relative to ordinary (spontaneous) Compton scattering when  $\tau_T < 1$  (Levich & Sunyaev 1970) and provides a heat input (rather than cooling) even when  $h\nu \ll kT_e$ . A high- $T_\nu$  radiation field can induce Compton scattering of the photons in the peak of the  $T_\nu$  distribution, shifting them to lower frequencies (Sunyaev 1971).

## 2.3 Cloud Assumptions

Assuming a standard solar composition (Grevesse & Anders 1989 is used by the code), we fix the total hydrogen density of the cloud gas at constant values  $n_H \gtrsim 10^{15} \text{ cm}^{-3}$  for which radiative processes dominate Compton scattering (Ferland & Rees 1988). We choose the condition of constant density rather than constant pressure because, as we explain below in Section 4, magnetic confinement of clouds allows a range of possible thermal pressures. The code reliably handles densities up to  $10^{18} \text{ cm}^{-3}$ , although then only at temperatures which are not too far below  $10^5 \text{ K}$ . Since individual clouds are always several orders of magnitude smaller than

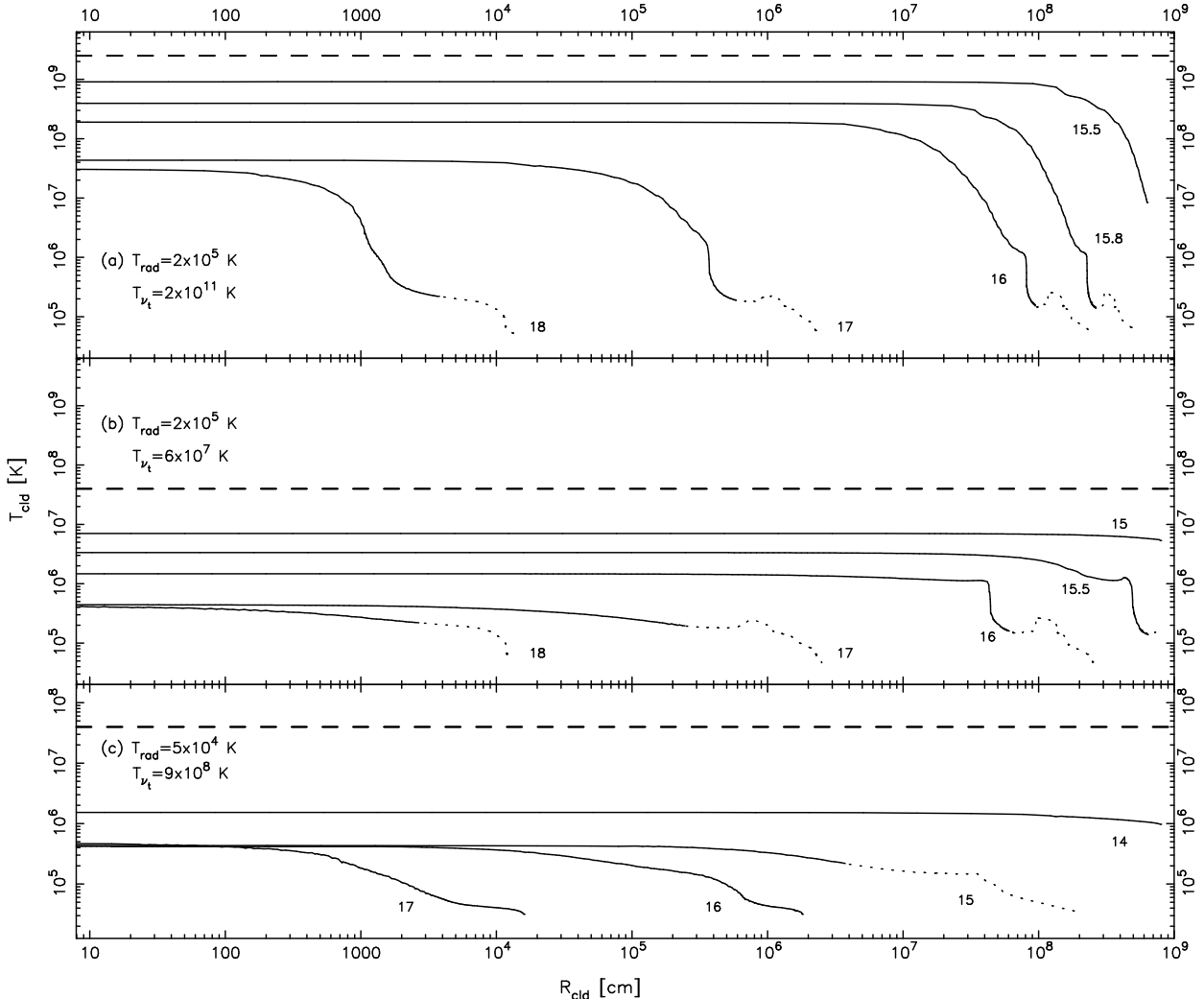


**Figure 1.** Cloud temperature  $T_{\text{cld}}$  plotted as a function of cloud depth  $R_{\text{cld}}$  at constant hydrogen density (log  $n_{\text{H}}$  indicated on each curve) for two limiting values of the radiation energy-density temperature  $T_{\text{rad}}$  and for different maximum radiation brightness temperatures  $T_{\nu_t}$ . The dashed line in each plot indicates the corresponding Compton temperature  $T_C$ . The dotted regions along the curves indicate where the cloud has an optical depth to free-free absorption that is greater than unity at 10<sup>15</sup> Hz.

the scalesize  $r$  of the source, a plane-parallel cloud geometry is an effective working approximation. The code then calculates the equilibrium electron temperature at discrete points separated by a thickness sufficiently small for the physical conditions within to be essentially uniform. The resulting cloud temperature  $T_{\text{cld}}$  is taken to be the equilibrium electron temperature in the final of these zones, at the far side (leading edge) of the cloud. Since the relative importance of all the radiative processes operating in a cloud depends upon the optical depth, the physical conditions vary from one point to the next. It is therefore necessary to examine the thermal structure of the clouds in order to identify the dominant processes as a function of depth  $R_{\text{cld}}$  into the gas.

### 3 THE THERMAL STRUCTURE OF A CLOUD

Fig. 1 shows log-log plots of  $T_{\text{cld}}$  as a function of  $R_{\text{cld}}$  for an isolated cloud of gas subjected to the primary radiation, at

the two limiting values of  $T_{\text{rad}}$ . The profile curves have been calculated up to a value of  $R_{\text{cld}}$  which either corresponds to a column density of at least 10<sup>23</sup> cm<sup>-2</sup> or is the maximum value allowed by the code for the specified density and radiation field. The dashed line in each plot indicates the Compton temperature,  $T_C$ , of the primary radiation field. In Fig. 1a, this is the initial  $T_C$ , since induced Compton scattering is important in this case, as we describe below. The dotted regions on the profiles indicate where the optical depth to free-free absorption at a frequency 10<sup>15</sup> Hz is greater than unity. For convenience, we use this criterion to distinguish between an ‘optically-thin’ and an ‘optically-thick’ cloud in the following. The most immediate result to be noted from these profiles is that they show there exist thermal and radiative equilibrium solutions for clouds of cool gas with very small scalesizes.

### 3.1 High Energy-Density Environments

The temperature profiles of an isolated cloud at various constant densities  $n_{\text{H}}$  and in a high  $T_{\text{rad}}$  environment are shown in Figs. 1a and 1b. These figures differ in the value of the self-absorption turnover frequency specified in the primary radiation field, with  $\nu_t = 3 \times 10^{13}$  Hz in Fig. 1a and with  $\nu_t = 5 \times 10^{14}$  Hz in Fig. 1b. These values correspond to radiation fields with a maximum brightness temperature  $T_{\nu_t} = 2 \times 10^{11}$  K and  $T_{\nu_t} = 6 \times 10^7$  K, respectively. In Fig. 1a, the initial Compton temperature of the radiation field is  $T_C = 3 \times 10^9$  K, which is considerably higher than  $T_C = 7 \times 10^7$  K for Fig. 1b owing to the additional contribution to Compton heating by induced scattering, which completely overwhelms ordinary (spontaneous) scattering in the high- $T_{\nu_t}$  case, but is negligible in the low- $T_{\nu_t}$  case.

#### 3.1.1 Optically-Thin Cloud

At densities  $\lesssim 10^{16}$  cm $^{-3}$ , the temperature of the gas at its illuminated edge approaches the Compton temperature. This is because as the density falls, collisional processes (free-free absorption, bremsstrahlung emission and collisionally-excited line emission) become increasingly less efficient and electron scattering makes an increasing contribution to the heating of the gas. Although free-free absorption accounts for essentially all of the heating at the highest densities and smallest  $R_{\text{cld}}$ , a comparison of the curves for  $\log n_{\text{H}} = 18$  in Figs. 1a and 1b shows that induced scattering is still capable of giving rise to a very high temperature (a few  $\times 10^7$  K) at the illuminated edge. At such high densities, however, induced scattering can only maintain the high temperatures over a short depth into the gas structure, since the free-free absorption rapidly depletes the energy in the FIR peak of the primary spectrum.

As the density falls below  $10^{16}$  cm $^{-3}$  and free-free absorption becomes negligible, the gas can remain at  $> 10^8$  K out to a column density where the optical depth to induced scattering at the FIR peak is of order unity. Beyond this depth, which is typically (a few  $\times 10^6$ )  $n_{16}^{-1}$  cm for the parameters in Fig. 1a (where  $n_{16} = n_{\text{H}}/10^{16}$  cm $^{-3}$ ), induced scattering begins to redistribute photons from the FIR peak. Consequently, the electron temperature gradually falls and approaches the value it would attain in the absence of induced scattering, as shown by the corresponding curves in Fig. 1b.

The cooling at densities  $\gg 10^{16}$  cm $^{-3}$  is chiefly regulated by collisional processes. At temperatures  $> 10^7$  K, the gas is very nearly completely ionized and consequently, the primary cooling occurs via free-free transitions (bremsstrahlung emission due to H and, to a lesser extent, He nuclei), giving rise to continuum X-ray radiation. Line radiation contributes typically  $\lesssim 30\%$  to the total radiative cooling in gas at these extreme temperatures. This radiation is chiefly comprised of atomic resonance lines arising from collisionally-excited Fe nuclei at ionization states XVI and above and re-emitted in the EUV band. As the temperature falls below  $10^7$  K, the lines are emitted by successively lower ionization states of Fe and the efficiency of bremsstrahlung decreases, although it remains the dominant coolant until  $T_{\text{cld}}$  falls below  $10^6$  K.

Gas with an initial temperature  $> 10^6$  K at its illu-

minated edge eventually cools to this temperature. There is a distinct break in the temperature profiles at the corresponding column density, indicating where the ionization level can no longer be maintained (see Fig. 1a and 1b at  $n_{\text{H}} < 10^{17}$  cm $^{-3}$ ). The lines which continue to cool the gas are emitted mainly by Fe in much lower ionization states (down to FeIX at 171 Å). These lines can account for up to 50% of the total radiative cooling in an optically-thin structure, dominating bremsstrahlung emission once the temperature falls below  $10^6$  K. The ionization front is most evident for  $\log n_{\text{H}} \lesssim 16$ , since the column densities attained before the gas appreciably cools are sufficiently large to trap the small cross-section, high-energy photons (at soft X-rays) that ionize the heavy element constituents. Photoabsorption of soft X-rays is an important source of heating for the gas as it passes through the ionization front. When the gas temperature at the illuminated edge is  $< 10^6$  K and hence, there is no ionization front (see Fig. 1b for  $\log n_{\text{H}} \gtrsim 17$ ), photoabsorption is important throughout the entire gas structure and provides an increasing contribution to the total heating, reaching up to 40% before the cloud becomes optically-thick.

At densities  $\gtrsim 10^{17}$  cm $^{-3}$ , radiative cooling is efficient enough to cool the gas to temperatures approaching  $10^5$  K before the structure becomes optically-thick. The cooling processes which become effective at these temperatures are collisionally-excited Ly  $\alpha$  line emission by HeII (304 Å), induced HII recombination and, at  $\log n_{\text{H}} = 18$ , MgVII (433 Å) line emission. In addition to H free-free absorption and photoabsorption of metals, about 10% of the total heating is due to collisional ionization of H from excited levels.

#### 3.1.2 Optically-Thick Cloud

As evident in Figs. 1a and 1b, dense gas in a high  $T_{\text{rad}}$  environment attains an optically-thick structure at temperatures typically just above  $10^5$  K. At the highest densities, the heating is entirely dominated by free-free absorption. Photoabsorption becomes significant for  $\log n_{\text{H}} \lesssim 17$  and gives rise to a distinctive peak in the corresponding temperature profiles. This peak does not emerge at the highest densities because line emission resulting from collisional excitations is efficient enough to cool the gas before it attains column densities sufficiently large for photoabsorption to become significant. The dominant lines are due to HeII (Ly  $\alpha$ , 304 Å), FeIX (171 Å) and MgVII (433 Å).

The peak is followed by a drop in the temperature towards  $10^5$  K, which is close to the ionization potentials of HII and HeII. At the corresponding depths, these nuclei contribute to the cooling of the gas through bremsstrahlung emission, recombination (including induced recombination of HII), HeII collisional ionization and Ly  $\alpha$  emission. Collisional ionization of heavier elements (mostly C, N, O) also contributes to the cooling. Although these processes regulate essentially all of the cooling of optically-thick gas when  $\log n_{\text{H}} \lesssim 17$ , they only account for up to about 30% of the total cooling of the whole structure since the line emission from optically-thin regions is far more efficient and therefore determines the overall cooling budget.

### 3.2 Low Energy-Density Environments

The temperature profiles of an isolated cloud of gas at various constant densities  $n_H$  and in a low  $T_{\text{rad}}$  environment are shown in Fig. 1c. These profiles are calculated for a radiation field with a Compton temperature  $T_C = 4 \times 10^7$  K and with a self-absorption turnover frequency  $\nu_t = 3 \times 10^{13}$  Hz, which is the same as that used in Fig. 1a, but corresponds to a maximum brightness temperature  $T_{\nu_t} = 9 \times 10^8$  K that is considerably lower owing to the lower energy density.

Here, the gas structure is always optically-thin above temperatures of a few  $\times 10^4$  K. The temperature of an optically-thin cloud at its illuminated face only begins to approach the Compton limit when the density falls well below  $10^{14}$  cm $^{-3}$ , with induced scattering contributing about 25% to the total Compton heating. At higher densities, essentially all the cloud heating is due to free-free absorption, although photoabsorption becomes important as the column density of the gas increases. The dominant cooling process at temperatures  $< 10^6$  K is line emission by collisionally-excited FeIX (171 Å) and, to a lesser extent, by collisionally-excited MgVII (433 Å) and OIV (789 Å). These lines can contribute up to 50% of the total cooling of the gas. As in the case for the profiles in Fig. 1b, HII and HeII nuclei regulate the cooling as the temperature approaches  $10^5$  K, the main processes being bremsstrahlung emission, recombination (including induced HII recombination), Ly  $\alpha$  emission and HeII collisional ionization. As the cloud thickness increases and the temperature drops below  $10^5$  K, heavier nuclei regulate both the cooling, through collisional ionizations, and the heating, through photoionization by soft X-rays.

#### 3.2.1 Summary

In this Section, we have presented a detailed study of the temperature and ionization structure of dense gas subjected to radiation that represents a typical primary source expected in the central continuum-forming region of AGN. We have examined and compared three different cases which encompass the high energy-density and the high brightness temperature regimes that are relevant to a primary radiation field in these central environments. The temperature profiles ( $T_{\text{cld}}$  vs.  $R_{\text{cld}}$ ) we have plotted show that cool temperatures and low column densities are indeed compatible thermal and radiative equilibrium properties of dense gas in the central regions of AGN. The dominant heating process is free-free absorption, while the cooling is chiefly due to collisionally-excited line emission.

In high energy-density environments, we have found that additional heating due to induced Compton scattering can make a significant difference to the internal ionization structure of optically-thin gas at even the highest densities, when the scattering competes with radiative (free-free) absorption. When the primary radiation field has a high brightness temperature, induced scattering effectively raises the temperature of gas by as much as two orders of magnitude at the illuminated edge of the structure. The gas is then able to cool efficiently through a much wider range of successively lower ionization stages of heavy nuclei. In low energy-density environments, the temperature and corresponding ionization levels of dense gas are below the potential of most metals, so that the line cooling is mainly due to hydrogen and he-

lium nuclei. Photoionization heating is also more important in this case.

## 4 THE THERMAL STABILITY OF A CLOUD

The solutions  $T_{\text{cld}}$  to the electron temperature evaluated at each point in a cloud of gas by balancing all the radiative heating and cooling processes under isochoric conditions describe thermal equilibria which can be either stable or unstable. The gas is said to be in a thermally stable phase if the response to a perturbation  $\delta T > 0$  is to immediately cool down. In other words, the criterion for thermal stability of a static gas is that the temperature derivative of the net volume cooling rate (i.e. total cooling  $C$  minus total heating  $H$ ) satisfies (Field 1965)

$$\frac{d(C - H)}{dT} > 0$$

at a local equilibrium temperature and under some physical constraint, such as the isochoric condition assumed here. An unstable equilibrium corresponds to a physical state in which the cloud gas is susceptible to perturbations that grow with time and eventually break up the gas into multiple stable sub-phases, thereby precluding the existence of clouds at that local equilibrium temperature.

It has been demonstrated that gas at temperatures above  $10^4$  K can exist in a thermally-stable state under the conditions expected in the BLR (McCray 1979; Krolik, McKee, & Tarter 1981; Guilbert, Fabian, & McCray 1983). Unlike this more distant gas, which is responsible for the optical and UV lines that characterize the spectra of radio-quiet AGN, photoionization and recombination do not regulate the overall thermal and ionization balance of denser gas distributed throughout the central source region. This is because at high densities and low column densities, free-free absorption dominates photoabsorption and collisional rates are faster than spontaneous recombination rates. It is not obvious, therefore, whether thermal instability precludes the existence of gas at the corresponding equilibrium temperatures which are found under these conditions.

Clearly, in this situation, the physical state of dense gas cannot be appropriately described using the standard photoionization parameter  $\xi = L/n_e r^2$  (where  $L$  is the ionizing luminosity), which assumes photoionization equilibrium. Hence, the thermal stability of the gas cannot be examined by plotting the corresponding radiative equilibrium curves ( $\xi$  vs.  $T_{\text{cld}}$ ). Instead, thermally unstable equilibria can be identified as solutions  $T_e$  to the equation  $C - H = 0$  at which the radiative cooling curve ( $C - H$  vs.  $T_e$ ) has a negative gradient, indicating that the local heating rate rises faster with temperature than does the local cooling rate. In general, such cooling curves have complex shapes as they trace the dominant processes for the corresponding temperature and ionization state of the gas.

The isochoric cooling curves for dense gas irradiated by a primary AGN source typically show thermally-stable equilibria over the range  $\sim 10^5$  K to  $\lesssim 10^6$  K and at temperatures above (a few)  $\times 10^6$  K (Kuncic 1996). It does not necessarily follow that these thermal and radiative equilibria are also stable under isobaric conditions, since there may be two or more combinations of  $(n_H, T_{\text{cld}})$  that correspond to

a given pressure, so that a multiphase equilibrium is possible. However, since the most plausible confinement mechanism for dense clouds in the central continuum-forming region of AGN is via magnetic stresses (CFR92), then the gas can maintain a range of possible thermal pressures while the total (thermal + magnetic) cloud pressure balances the total external pressure (which is likely to be magnetically-dominated – see Kuncic, Blackman, & Rees 1996). Thus, isobaric instability at a fixed thermal pressure does not preclude the existence of the type of clouds in question here. On the other hand, we note that magnetic confinement does not alleviate isochoric instability.

The same may also hold for the more distant BLR clouds, where magnetic fields may contribute a substantial fraction to the external pressure if additional heating mechanisms in the hot, intercloud plasma are unable to provide the large thermal pressures required to maintain pressure equilibrium with the clouds (Mathews & Ferland 1987). Typical cooling curves for the photoionized gas which comprises the BLR clouds in this region indicate that equilibrium temperatures  $\sim 10^5$  K may be isobarically unstable (see Figs. 2 and 3 in Krolik, McKee, & Tarter (1981), for example). However, if these clouds are magnetically-confined (Rees 1987) and can thereby maintain a range of possible pressures, then there is a corresponding range of possible stable phases. Indeed, this may even explain the wide range of reprocessing features (e.g. warm absorber, broad absorption lines) that are inferred to originate from roughly the same region ( $\sim 0.1$ – $1$  pc).

## 5 EMERGENT SPECTRA FROM A DISTRIBUTION OF CLOUDS

In the previous Sections, we have examined how very dense gas subjected to an intense radiation field, representing a typical primary AGN source, can cool to temperatures substantially lower than the Compton value before becoming Thomson thick. It is now of particular interest to predict the emergent spectra from a source region containing such cool, dense substructure and to then compare these spectra with current observations in an attempt to test the hypothesis that these reprocessing clouds may indeed exist in the central regions of AGN.

The simplest method is to combine the emission from a homogeneous distribution of individual clouds into a composite spectrum which can then be directly compared with observed spectra (Netzer 1990). In addition to the parameters required to model an isolated cloud ( $n_{\text{H}}$ ,  $R_{\text{cld}}$ ) in a prescribed radiation field, a volume filling factor  $f$  must also be specified. We have constructed a detailed model for such a cloud system; this is described next, followed by a comparison of the predicted emergent spectra with current observations.

### 5.1 The Cloud Model

Adopting the method of FR88, we assume that homogeneous, dense clouds embedded within a plane-parallel source region of size  $R$  absorb and reprocess the primary radiation emitted by surrounding relativistic particles. We are particularly interested in the specific scenario of many small-

scale clouds which occupy only a tiny fraction  $f$  of the total volume, but which reprocess a significant fraction of the primary radiation. Hence, we assume a covering factor of unity, so that there is at least one cloud along every line of sight. In this picture, the volume filling factor is equivalent to the line of sight filling factor, with  $f = \mathcal{N}_{\text{los}} R_{\text{cld}} / R$ . The total number of clouds along the line of sight,  $\mathcal{N}_{\text{los}}$ , is defined by specifying a total line of sight hydrogen column density  $N_{\text{tot}} = \mathcal{N}_{\text{los}} n_{\text{H}} R_{\text{cld}}$  (a quantity that can be observationally constrained). The opacity of a cloud,  $\kappa_{\nu}$ , then implies a total line of sight optical depth for the system,  $\tau_{\nu} = \mathcal{N}_{\text{los}} \kappa_{\nu} R_{\text{cld}}$ .

The emergent spectrum from the source region is calculated by integrating the source function  $S_{\nu}$  weighted by the optical depth, as prescribed by the Schwarzschild-Milne solution to the plane-parallel radiative transfer equation,

$$F_{\nu} = 2 \int_0^{\tau_{\nu}} dt_{\nu} S_{\nu}(t_{\nu}) E_2(t_{\nu}),$$

where  $E_2(t) = e^{-t} - tE_1(t)$  is the standard exponential integral function (of second-order) and where the first-order function  $E_1(t) \equiv \int_t^{\infty} dt' t'^{-1} e^{-t'}$  is calculated with a numerical integration. Since the clouds are assumed to be the only source of opacity, the source function for the region can be expressed as

$$S_{\nu} = \frac{(1-f)\epsilon_{\nu}^{\text{prim}}}{f\kappa_{\nu}} + S_{\nu}^{\text{cld}},$$

where  $\epsilon_{\nu}^{\text{prim}}$  is the (constant) volume emissivity of the primary radiation and  $S_{\nu}^{\text{cld}}$  is the cloud source function, which explicitly includes line emission (this was not taken into account by FR88). A gaussian profile is used for the lines, assuming the clouds are in random motion with a bulk velocity  $V \sim 0.2c$ , which is of the order of the free-fall velocity at about 20 gravitational radii.

With homogeneous clouds, the emergent spectrum simplifies to

$$F_{\nu} = \left( \frac{F_{\nu}^{\text{prim}}}{2\tau_{\nu}} + S_{\nu}^{\text{cld}} \right) [1 - 2E_3(\tau_{\nu})],$$

where  $F_{\nu}^{\text{prim}} = 2(1-f)\epsilon_{\nu}^{\text{prim}}R$  is the (optically-thin) flux of the primary radiation field.

The attenuation described by the (third-order) exponential function  $E_3(\tau_{\nu})$  converges in the limit of large and small optical depth according to

$$1 - 2E_3(\tau_{\nu}) \sim \begin{cases} 2\tau_{\nu}, & \tau_{\nu} \ll 1 \\ 1, & \tau_{\nu} \gg 1. \end{cases}$$

This behaviour implies corresponding regimes in the equation for the emergent spectrum,

$$F_{\nu} \sim \begin{cases} F_{\nu}^{\text{prim}} + \mathcal{N}_{\text{los}} F_{\nu}^{\text{cld}} & \tau_{\nu} \ll 1 \\ F_{\nu}^{\text{prim}}/2\tau_{\nu} + S_{\nu}^{\text{cld}} & \tau_{\nu} \gg 1, \end{cases}$$

where  $F_{\nu}^{\text{cld}} = S_{\nu}^{\text{cld}}[1 - 2E_3(\kappa_{\nu} R_{\text{cld}})]$  is the flux emitted by a typical cloud. The source region is optically-thin to absorption ( $\tau_{\nu} \ll 1$ ) in the EUV band (as well as in the hard X-ray band, where the primary radiation remains unattenuated). The contribution by  $\mathcal{N}_{\text{los}}$  clouds to the emergent spectrum is just the sum of their optically-thin spectra (chiefly due to lines and some bremsstrahlung). Since individual clouds are optically-thick at and below the FIR band, the reprocessed spectrum due to many clouds always emerges as a complete

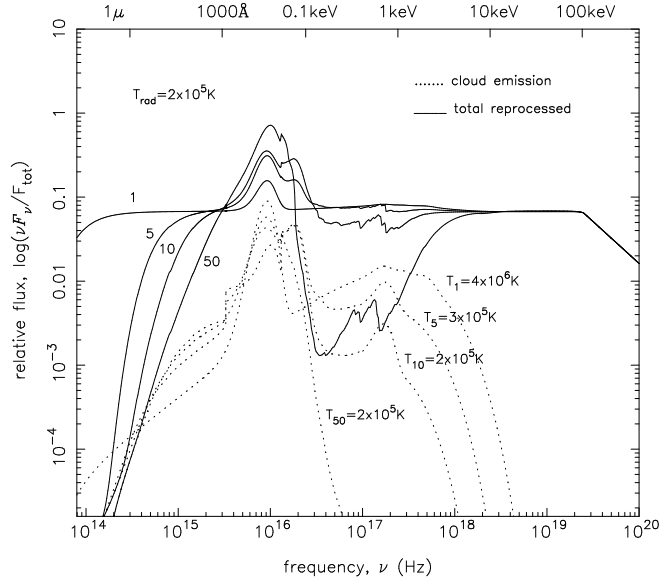


**Figure 2.** Emitted and total reprocessed (attenuated primary + cloud emission) spectra from a typical cloud along lines of sight with 1, 5, 10 and 50 identical clouds. The corresponding cloud temperature is indicated.

blackbody (in the Rayleigh-Jeans limit) at these frequencies (i.e.  $\tau_\nu \gg 1$ ). At intermediate values of  $\tau_\nu$ , the emergent spectrum depends more sensitively on the total number of clouds; the optical depth to absorption at optical/UV frequencies and at soft X-ray energies increases with  $N_{\text{los}}$ .

A direct iteration of the cloud source function  $S_\nu^{\text{cld}}$  is strictly required for self-consistency with the emergent spectrum when  $N_{\text{los}} \gg 1$ . We approximate  $S_\nu^{\text{cld}}$  by taking into account that a typical cloud does not ‘see’ all of the primary radiation, owing to shielding by other clouds, which generate a local reprocessed radiation field. Assuming the filling factor and intercloud medium are uniform, the fraction of primary radiation seen by a cloud is approximately  $d/R = 1/N_{\text{los}}$ , where  $d$  is the smallest region in which there is one cloud along every line of sight.

Using CLOUDY, we construct a working grid model in which the spectrum incident upon a cloud along a line of sight with a total of  $N_{\text{los}}$  clouds is taken to be

$$F_\nu^{\text{inc}} = \left( \frac{1}{N_{\text{los}}} \right) F_\nu^{\text{prim}} + \left( 1 - \frac{1}{N_{\text{los}}} \right) F_\nu^{\text{repr}},$$

where  $F_\nu^{\text{repr}}$  is the reprocessed flux (attenuated primary plus emitted thermal) generated by  $N_{\text{los}} - 1$  clouds. We then take  $S_\nu^{\text{cld}}$  to be the source function of the cloud irradiated with this incident spectrum. The assumption of a covering factor of unity implies that the only primary radiation ‘seen’ directly is that which is transparent to radiative absorption (this will be at hard X-ray energies). However, it is conceivable that the region is not homogeneous and that there could be some primary radiation emitted in an outer boundary layer where clouds are too few in number to absorb the soft X-rays. In any case, it is straightforward to take into account that a fraction of the primary radiation may be generated in regions which do not intercept any reprocessing material.

Our procedure gives a much more accurate treatment than that of FR88, where the spectral properties (opacity and emissivity) of the reprocessing gas were taken to be

those calculated for an isolated cloud irradiated by the primary source (i.e. without considering the local reprocessed field). As a consequence of our treatment, the internal temperature gradient in each cloud is significantly lower than that in the case of an isolated cloud, as examined in Section 3 (and see in particular the temperature profiles in Fig. 1a). Similarly, the spectral properties and emergent flux from successive clouds converge towards local thermodynamic equilibrium as more of the radiation is reprocessed.

In Fig. 2, we plot the spectra emerging from lines of sight with different total numbers of optically-thin clouds that are irradiated by an incident spectrum  $F_\nu^{\text{inc}}$  as defined in this grid model. The clouds are identical, with  $n_{\text{cld}} = 10^{18} \text{ cm}^{-3}$  and  $R_{\text{cld}} = 1 \times 10^3 \text{ cm}$ , and the primary radiation field is the same as that assumed in Fig. 1a, for which isolated clouds have the largest internal temperature gradient. The dotted curves are the spectra emitted by a cloud along lines of sight with  $N_{\text{los}} = 1, 5, 10, 50$ . The solid curves represent the corresponding total reprocessed spectra obtained by summing the attenuated primary flux with the emitted flux.

This plot shows how thermal coupling with the local reprocessed radiation field generated when  $N_{\text{los}} \gg 1$  gives rise to much cooler clouds than when  $N_{\text{los}} = 1$ . Because of the much higher values of  $T_{\text{cld}}$ , the spectrum emitted by an isolated, optically-thin cloud along a line of sight is chiefly due to bremsstrahlung and line radiation at soft X-ray and EUV energies. As  $N_{\text{los}}$  increases and  $T_{\text{cld}}$  converges toward  $T_{\text{rad}}$ , however, the emission spectrum of a typical cloud along the line of sight becomes increasingly less important at soft X-ray energies and approaches a blackbody at low frequencies. The emission is in the UV, where the Ly edge emerges, and in the EUV, where the heavy element lines emerge. These are the only spectral ‘windows’ from which the reprocessed radiation can emerge, since thermal self-absorption prevails at lower frequencies where the optical depth to free-free ab-

sorption is  $\gg 1$ , while photoabsorption depletes the primary soft X-rays, which cannot be replenished by thermal emission owing to the decrease in  $T_{\text{cld}}$ . The hard X-rays remain unattenuated since there is no Compton scattering.

## 5.2 Results

Plots of the predicted emergent spectra are presented in Figs. 3, 4 and 5. The primary spectrum defined in Section 2 is shown for reference in each figure (dash-dot line) and has the same  $T_{\text{rad}} = 2 \times 10^5$  K in Figs. 3 and 4, but with  $\nu_t = 3 \times 10^{13}$  Hz and  $\nu_t = 5 \times 10^{14}$  Hz, respectively, while Fig. 5 has  $T_{\text{rad}} = 5 \times 10^4$  K, with  $\nu_t = 3 \times 10^{13}$  Hz. The spectra are plotted as flux per logarithmic frequency interval,  $\nu F_\nu$ , relative to the total integrated flux,  $F_{\text{tot}} = acT_{\text{rad}}^4$ , thus giving the best indication of the frequency ranges where most of the radiation is absorbed and reemitted by the clouds. Also shown in the figures is a hypothetical power-law from the optical (2500 Å) to X-ray (2 keV) with a spectral index  $\alpha_{\text{ox}}$  that is taken from current observations (Puchnarewicz et al. 1996), as well as the slope of the observed optical spectra (taken from the same data), where the blue bump component is strongest. In Fig. 5b, the optical to X-ray power-law is drawn relative to 2 keV X-rays in the primary spectrum, owing to the lack of flux in the reprocessed spectrum. This power-law therefore indicates the maximum relative flux in the optical/UV in this spectrum.

The spectra shown in each plot are calculated for a constant value of  $n_{\text{H}}$ . The solid and dotted curves in Figs. 3 and 4 distinguish between small and large values of  $R_{\text{cld}}$ , respectively, that correspond to clouds which are optically-thin and optically-thick to free-free absorption at  $10^{15}$  Hz, as examined in Section 3. The lower panels in these figures show spectra for lower values of  $N_{\text{tot}}$  that correspond to a single optically-thick cloud ( $N_{\text{los}} = 1$ ), so the emergent spectra closely resemble that expected for a ‘slab’ (since the covering factor is implicitly assumed to be unity) and can be directly compared with the spectra calculated for smaller  $R_{\text{cld}}$  and higher  $N_{\text{los}}$ . Fig. 5a also shows the integrated spectrum due to a single cloud along the line of sight, while Fig. 5b shows the corresponding spectrum for  $N_{\text{los}} = 100$ . The parameters used in Fig. 5c are specifically chosen to represent the Thomson-thin, free-free emission model proposed by Barvainis (1993) for the optical/UV blue bump component in AGN spectra.

### 5.2.1 Interpretation

The predicted emergent spectra clearly exhibit the common property of an energetically-significant reprocessed component which results from the direct reradiation of energy that has been depleted from the primary radiation field in the optical/UV band and below (by free-free absorption and in some cases, induced Compton scattering) and also in the soft X-ray band (by photoabsorption). A Rayleigh-Jeans component ( $\propto \nu^2$ ) emerges when free-free absorption has appreciably depleted the low-frequency primary radiation (see the upper panels in Figs. 3 and 4 and also Figs. 5a and 5b).

Photoabsorption of soft X-rays becomes the chief heating mechanism for dense gas once the low-frequency radiation is efficiently removed. This is demonstrated by comparing the spectra in Fig. 3b with those in Fig. 3a, which are

calculated for lower  $n_{\text{H}}$  and higher values of  $N_{\text{tot}}$ , but which exhibit less absorption of the primary soft X-rays because not all of the low-frequency photons have been removed.

The difference in gas temperatures is also an important factor determining the relative importance of free-free absorption and photoabsorption. Below  $\sim 10^5$  K, when the ionization state is lower and hence, there are fewer free electrons, photoabsorption can be stronger than free-free absorption. This is evident in Fig. 5. Similarly, the soft X-ray extinction also becomes appreciable when the primary radiation field has less low-frequency energy available for free-free absorption. This is demonstrated by comparing Fig. 3 with Fig. 4, which is for a higher FIR turnover frequency,  $\nu_t$ , and which shows how less energy in the primary spectrum available for low-frequency heating is compensated for by more soft X-ray photoelectric heating.

The photoabsorption spectral features which emerge most notably are L-edges of C and O ( $\sim 0.4$  keV) and in some cases, an Fe K-edge in the X-ray band ( $\sim 0.8$  keV) and a Ly edge due to collisional ionization of HeII (228 Å). Probably the most striking result shown by these spectra, however, is that for all feasible cloud parameters, line radiation is significant and in most cases dominates the continuum radiation. The bulk of the predicted lines emerge in the EUV band, which is the only ‘window’ in the broadband spectra that is unaffected by radiative absorption due to the clouds. All the lines are collisionally-excited heavy element lines (spontaneous recombination radiation is negligible by comparison, as discussed earlier in Section 4), with the most energetically-significant lines typically being FeIX (171 Å), HeII (304 Å) and MgVII (433 Å).

In the high  $T_{\text{rad}}$  case (Figs. 3 and 4), almost all the lines are resonance lines of Fe in various ionization states and the total line emission dominates the continuum emission both when there are many optically-thin clouds and when there are fewer optically-thick clouds at the same total column density. This is because in such an intense radiation field, line emission is the most efficient means by which the clouds can cool from temperatures which are initially very high. The case when optically-thin clouds are insufficient in number to reprocess an energetically-significant amount of radiation and thereby cool appreciably is illustrated in Fig. 3b, with  $N_{\text{tot}} = 4 \times 10^{22} \text{ cm}^{-2}$  (solid curve). The temperature of the optically-thin clouds is so hot ( $\sim 10^{6.8}$  K) that a hump emerges at X-ray energies due to bremsstrahlung emission and indeed, this exceeds the line emission. The spectrum of the thicker clouds (dotted curve) shows the lines responsible for their much cooler temperature ( $\sim 10^{5.5}$  K).

In the low  $T_{\text{rad}}$  case shown in Fig. 5, fewer Fe lines are emitted owing to the lack of high-ionization state Fe ions. The collisionally-excited HeII (304 Å) line, on the other hand, is a prominent feature as is the HeII Lyman (228 Å) edge due to collisional ionization. A H Ly edge is also visible either in absorption or, at higher  $N_{\text{tot}}$ , in emission (compare Figs. 5a and 5b). This edge emerges because the cloud temperature is below  $10^5$  K and free-free absorption is incapable of thermalizing the spectrum at optical frequencies when  $N_{\text{tot}}$  is low.

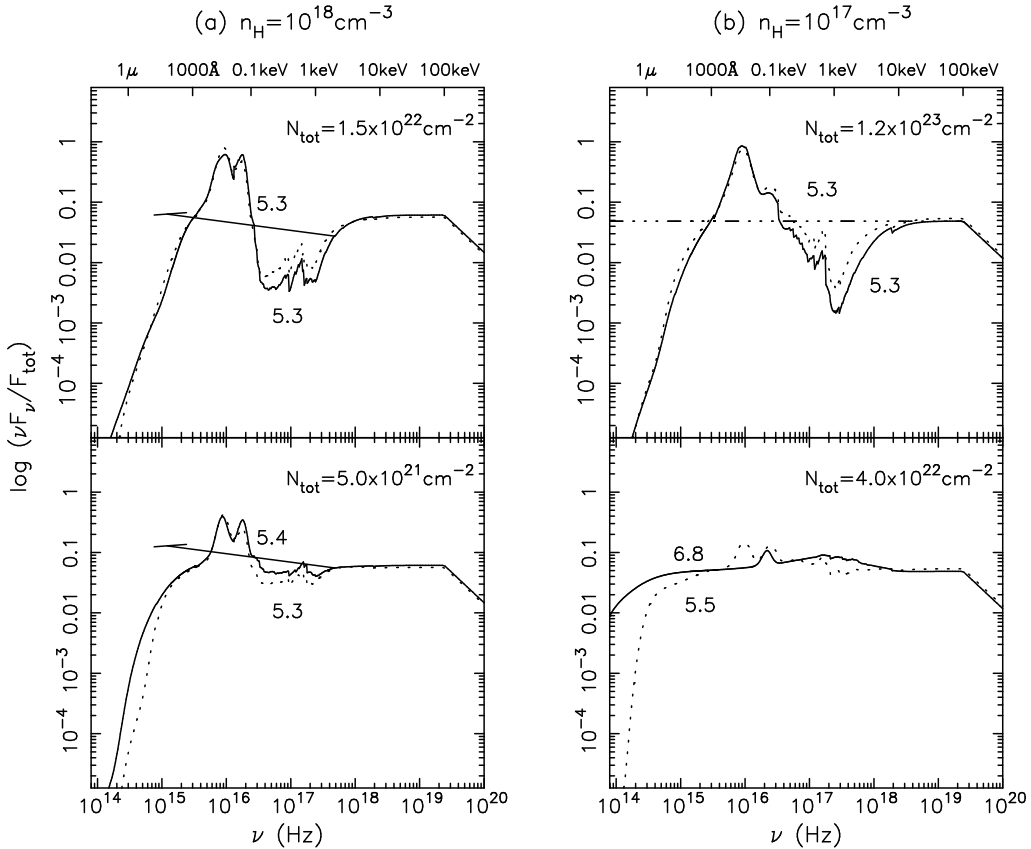


**Figure 3.** Emergent spectra from a source region in which primary radiation with an energy-density temperature  $T_{\text{rad}} = 2 \times 10^5$  K and with a maximum brightness temperature  $T_{\nu_t} = 2 \times 10^{11}$  K is reprocessed by a total line-of-sight column density  $N_{\text{tot}}$  of homogeneous clouds with density  $n_{\text{H}}$  and size  $R_{\text{cld}}$ , where (a)  $R_{\text{cld}} = 1 \times 10^3$  cm,  $5 \times 10^3$  cm; and (b)  $R_{\text{cld}} = 2 \times 10^5$  cm,  $4 \times 10^5$  cm (the total line-of-sight number of clouds is  $\mathcal{N}_{\text{los}} = N_{\text{tot}}/n_{\text{H}}R_{\text{cld}}$ ). Small and large  $R_{\text{cld}}$  are distinguished by solid and dotted curves, respectively, and the logarithm of the resulting cloud temperature,  $\log T_{\text{cld}}$  is indicated. Also shown is a hypothetical power-law indicating the relative fluxes of the optical/UV and X-ray bands using a spectral index  $\alpha_{\text{ox}} = 1.14$  obtained from recent observations. The average observed optical/UV slope is also indicated. The dash-dots line represents the primary spectrum.

### 5.2.2 Testing the Free-Free Emission Model

Fig. 5c illustrates a specific case using parameters representative of an optically-thin thermal model proposed by Barvainis (1993). In this model, the optical/UV blue bump component is attributed to thermal bremsstrahlung emission by a source region that is occupied by clouds with  $\mathcal{N}_{\text{los}} \sim 1$  and that is optically-thin to free-free absorption above optical frequencies. The main shortcoming of this model is that it is based on an analytical treatment in which free-free emission is assumed to be solely responsible for the blue bump. The cloud parameters (temperature and size) are therefore not calculated under thermal and radiative equilibrium conditions and hence, are not self-consistent with the ionization balance of the gas and the ambient reprocessed radiation field. By taking this into account, our results demonstrate that free-free radiation is not the dominant component of the emission from the gas, owing to significant contributions by bound-free and bound-bound (line) emission. For the representative parameters of this model, we find that photoionization contributes up to 35% of the total heating budget (this is evident in the predicted spectrum in Fig. 5c), while the total cooling budget is dominated by line emission,

which accounts for up to 3 times more than the continuum emission. We find that this line-to-continuum ratio is even higher when the clouds are thinner and  $\mathcal{N}_{\text{los}} \gg 1$ . Similar results demonstrating the inadequacies of free-free models for the blue bump have also been obtained by Collin-Souffrin et al. (1996).

### 5.2.3 Comparison with Observations

The predicted emergent spectra in Figs. 3, 4 and 5 indicate that reprocessing by very dense, small-scale clouds is energetically-significant under a wide range of conditions. However, when compared with observed AGN spectra, such as those presented in the atlas of SEDs by Elvis et al. (1994), the predicted spectra show an obvious lack of flux over a narrow, but crucial range of optical/UV energies below 10 eV (above  $\sim 1200$  Å), where the blue bump component reaches a maximum and appears to roll over. The same problem can be seen with the spectra predicted by the model of FR88 (see their Fig. 8).

The discrepancy can be described quantitatively with the parameter  $\alpha_{\text{ox}}$ , which is usually defined as the slope of

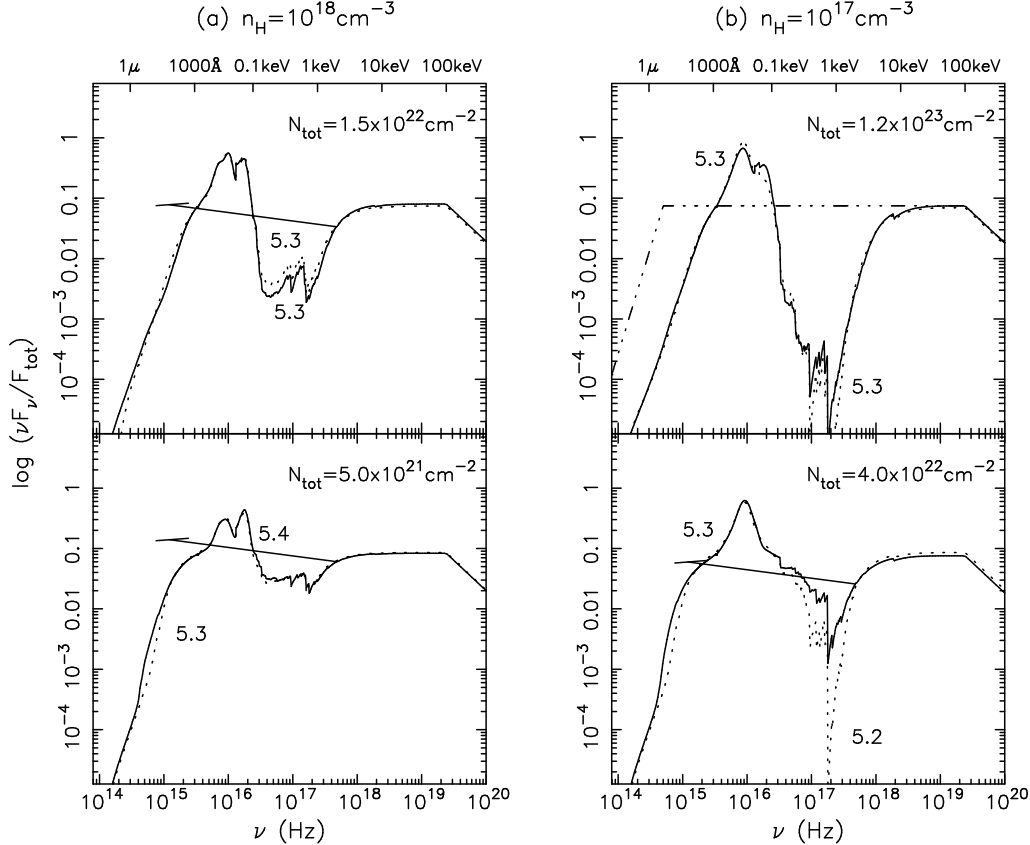


**Figure 4.** Emergent spectra from a source region in which primary radiation with an energy-density temperature  $T_{\text{rad}} = 2 \times 10^5$  K and with a maximum brightness temperature  $T_{\nu_t} = 6 \times 10^7$  K is reprocessed by a total line-of-sight column density  $N_{\text{tot}}$  of homogeneous clouds with density  $n_{\text{H}}$  and size  $R_{\text{cld}}$ , where (a)  $R_{\text{cld}} = 1 \times 10^3$  cm,  $5 \times 10^3$  cm; and (b)  $R_{\text{cld}} = 2 \times 10^5$  cm,  $4 \times 10^5$  cm (the total line-of-sight number of clouds is  $N_{\text{los}} = N_{\text{tot}}/n_{\text{H}}R_{\text{cld}}$ ). Small and large  $R_{\text{cld}}$  are distinguished by solid and dotted curves, respectively, and the logarithm of the resulting cloud temperature,  $\log T_{\text{cld}}$  is indicated. Also shown is a hypothetical power-law indicating the relative fluxes of the optical/UV and X-ray bands using a spectral index  $\alpha_{\text{ox}} = 1.14$  obtained from recent observations. The average observed optical/UV slope is also indicated. The dash-dots line represents the primary spectrum.

a hypothetical power-law ( $F_{\nu} \sim \nu^{-\alpha}$ ) extending over 2500 Å-2 keV (Tananbaum et al. 1979), giving a measure of the relative optical to X-ray flux and thus, a measure of the strength of the blue bump component. This power-law is drawn against some of the predicted spectra for comparison. The spectral index used is  $\alpha_{\text{ox}} = 1.14$ , which is the mean value measured from the Rosat International X-ray/Optical Survey (RIXOS) of AGN (Puchnarewicz et al. 1996). Note, however, that we have not included any reprocessed component in X-rays, which could flatten the 2-40 keV spectrum. Also shown is the average slope measured in the optical band, with  $\alpha_{\text{opt}} \sim 0.92$  from the same sample. The inconsistency between our predicted spectra and the observed optical/UV spectra is even more apparent when considering that the RIXOS sample of AGN is considerably larger and less selective than other samples, which typically show steeper optical to X-ray ratios, with an average  $\alpha_{\text{ox}} \sim 1.4$  (e.g. the optically-selected PG quasars analysed by Elvis et al. 1994).

In the high  $T_{\text{rad}}$  case (Figs. 3 and 4), the emergent spectra are typically flux-limited in the optical/UV due to the large line of sight optical depths to free-free absorption at these frequencies. The blackbody spectra clearly rise too

steeply and lack the flux required to account for the peak in the blue bump. This deficiency is apparent also when the spectra are optically-thin at these frequencies (see Fig. 3b, lower panel), since free-free absorption then reprocesses very little of the primary radiation and photoabsorption reprocesses even less, so that very little flux is reemitted in the optical/UV band.

The closest agreement with the observed optical/UV spectra is found in the low  $T_{\text{rad}}$  case shown by Fig. 5a. However, the conditions in this case are quite different from those which initially motivated our investigation. Free-free absorption is less efficient (since there are fewer free electrons), so that most of the primary radiation is reprocessed by photoabsorption, with the soft X-rays reemitted as optical/UV radiation. At higher  $N_{\text{tot}}$ , atomic absorption depletes the X-rays towards harder energies and the spectrum approaches a complete blackbody, as can be seen in Fig. 5b. This spectrum shows that even if some of the primary X-rays are replenished in an outer boundary layer of the source region (where there are essentially no clouds in these conditions), the ratio of the optical/UV to X-ray flux is still inconsistent

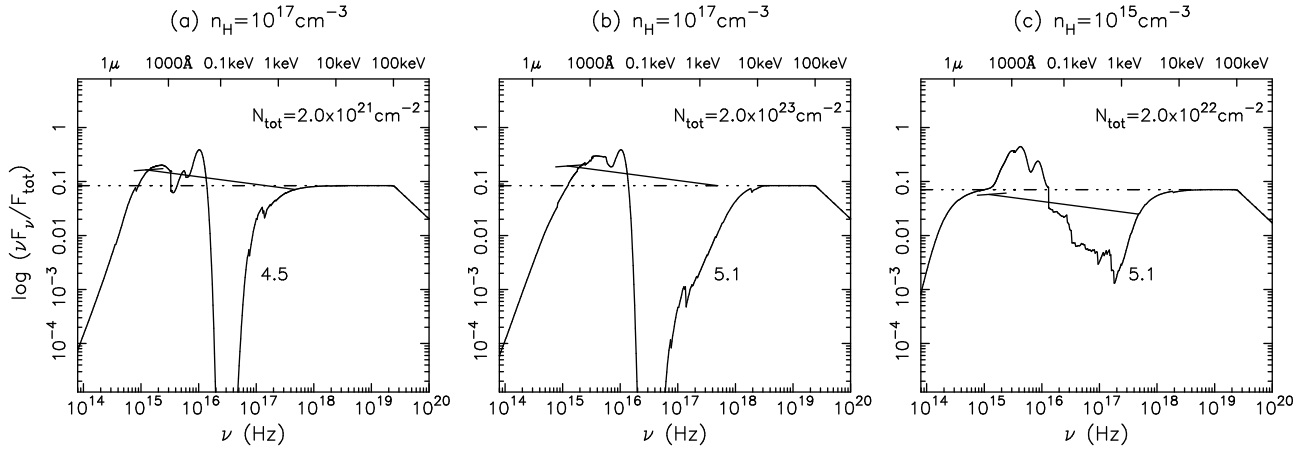


**Figure 5.** Emergent spectra from a source region in which primary radiation with an energy-density temperature  $T_{\text{rad}} = 5 \times 10^4$  K and with a maximum brightness temperature  $T_{\nu t} = 9 \times 10^8$  K is reprocessed by a total line-of-sight column density  $N_{\text{tot}}$  of homogeneous clouds with density  $n_{\text{H}}$  and size  $R_{\text{cld}}$ , where (a)  $R_{\text{cld}} = 2 \times 10^4$  cm; (b)  $R_{\text{cld}} = 2 \times 10^4$  cm; and (c)  $R_{\text{cld}} = 2 \times 10^7$  cm (the total line-of-sight number of clouds is  $N_{\text{los}} = N_{\text{tot}}/n_{\text{H}}R_{\text{cld}}$ ). The logarithm of the resulting cloud temperature,  $\log T_{\text{cld}}$  is indicated. Also shown is a hypothetical power-law indicating the relative fluxes of the optical/UV and X-ray bands using a spectral index  $\alpha_{\text{ox}} = 1.14$  obtained from recent observations. The average observed optical/UV slope is also indicated. The dash-dots line represents the primary spectrum.

with the observations. The spectrum rises too steeply at the frequencies where the blue bump typically peaks.

It thus appears that consistency with the blue bump requires a total line of sight optical depth to free-free absorption that is not large at optical/UV energies, so that the flux is not blackbody-limited. At the same time, some photoabsorption is required to produce an energetically-significant reprocessed component in the optical/UV.

The only band that remains optically-thin to radiative absorption (apart from hard X-rays) is the EUV, where the bulk of the radiation reprocessed by the clouds emerges as extremely broad lines. Although most extragalactic objects are virtually impossible to detect at EUV energies because of strong galactic absorption by interstellar gas, recent observations have been successful in identifying many AGN in directions of low galactic neutral hydrogen as EUV sources (see Fruscione 1995 and references cited therein).

For some objects, such as the radio-quiet quasars Ton S 180 and H1821+643, the observed spectra at either end of the EUV clearly exhibit both a blue bump that turns over at  $\lesssim 10$  eV and a steep soft X-ray excess at  $\lesssim 0.5$  keV and the indication is that the optical/UV to soft X-ray must be comprised of two or more components (Wisotzki et al. 1995; Kolman et al. 1993). To date, however, very few EUV and soft X-ray observations have been undertaken simultaneously and so the spectral slope into the EUV and its connection with the lower and higher energy bands remains poorly known. Such observations of the Seyfert galaxy Mrk 841 have revealed a soft X-ray spectrum that extrapolates with a power-law fit well into the EUV. This adds further support to the implication from non-simultaneous observations that the bulk of the spectral power peaks in the EUV band (Nandra et al. 1995) and that it is connected to the soft X-rays, possibly forming a single ‘big bump’ component that extends over to the optical/UV, where it con-

nnects with the blue bump (Walter & Fink 1993). Very recent results from RIXOS are also consistent with this idea (Puchnarewicz et al. 1996).

Observations of the Seyfert 1 galaxy NGC 5548 show possible broad, weak EUV lines that are difficult to explain in the framework of photoionization models (Kaastra, Roos, & Mewe 1995 – but see also Marshall, Carone, & Peterson 1996). Consequently, it has been suggested that they are instead due to a dense, collisionally-ionized warm absorber, with the emitting material then most likely being in the form of many small clouds. This fits in with the idea of a ‘very broad line region’ (VBLR) containing highly-ionized material, as proposed by Ferland, Korista, & Peterson (1990) in order to explain similar broad-base lines observed in other AGN. The line widths place the emitting region in the inner BLR. In a global picture, it is plausible that the entire nuclear region of radio-quiet AGN contains various forms of thermal reprocessing material with radiative properties determined by the prevalence of photoionization equilibrium in the BLR, while collisional processes become increasingly more important in the denser, more central regions.

### 5.3 Summary and Discussion

We have presented a detailed analysis of very dense, geometrically-thin clouds that may exist in the central continuum-forming region of AGN and that reprocess the primary radiation generated therein. We have employed numerical methods to examine their physical properties under thermal and radiative equilibrium conditions. It was found that very dense gas can readily achieve cool temperatures before reaching large column densities, which is consistent with the idea of filaments or sheets confined by an external magnetospheric environment. The heating of the gas is

dominated by free-free absorption, although photoabsorption can be important depending on the amount of primary radiation available at low-frequencies and also on the amount of available free electrons.

We have found that the total cooling budget is dominated by collisionally-excited line radiation, essentially all of which is emitted in the EUV band, which remains transparent to radiative absorption at the column densities we considered. We have also discussed the thermal stability of the gas in relation to that of other reprocessing gas residing in more distant regions. While there may be some thermal and radiative equilibria which are unstable under isochoric or isobaric conditions, magnetic confinement allows a much wider range of possible pressures, so that there is always likely to be some stable equilibria.

We have calculated the emergent spectra from a source region in which the primary continuum radiation is generated and in which dense clouds are distributed homogeneously. These spectra show that along lines of sight which are Thomson-thin, dense clouds are capable of reprocessing an energetically-significant amount of the primary radiation generated in the central continuum-forming region of AGN. However, our predicted spectra show that when dominated by free-free absorption, this reprocessing cannot solely be responsible for the observed optical/UV emission that is identified as the blue bump.

When the total line of sight optical depth to free-free absorption is large at the crucial optical/UV frequencies where the blue bump peaks, the emergent flux is blackbody-limited. This is particularly the case for high energy-density environments, since the large supply of free electrons ensures that reprocessing by very dense, Thomson-thin gas is dominated by free-free absorption. In low energy-density environments, the reprocessing is largely due to photoabsorption and the optical/UV emission more closely resembles the blue bump provided again that the spectrum is not completely blackbody at these crucial frequencies. This is consistent with recent results that suggest reprocessing by Thomson-thick clouds can produce spectra which can account for the blue bump as well as soft X-ray excesses and an X-ray reflection feature (Collin-Souffrin et al. 1996). Because these Thomson-thick clouds are less dense, free-free absorption is not important above IR frequencies and the optical/UV spectrum where the blue bump peaks is entirely dominated by free-bound emission, rather than being blackbody-limited as is the case here. In the presence of strong photoabsorption, however, a covering factor of unity requires the primary radiation to be generated in an outer layer of the source region that is essentially free of this type of clouds, so that some of the primary soft X-rays are detected (but see also Collin-Souffrin et al. 1996). A few hotter, thinner clouds in this outer layer would also contribute to the observed soft X-ray emission.

Realistically, reprocessing clouds at the centres of AGN are probably distributed inhomogeneously, with a range of densities and temperatures, so that different lines of sight have different column densities and different optical depths to radiative absorption and Thomson scattering. Indeed, there is growing evidence that the BLR contains such a mixture of optically-thin and optically-thick cloud structure, contrary to long-standing ideas (Shields, Ferland, & Peterson 1995).

Despite the inability of very dense, Thomson-thin clouds to account for the blue bump, the reprocessed spectra can still provide a significant contribution to the SED of radio-quiet AGN. The bulk of the radiation that is reprocessed by the clouds examined here emerges as very broad EUV lines, which form the most prominent and energetically-dominant spectral feature. This result is particularly interesting in light of the current observations which are now for the first time identifying radio-quiet quasars and Seyferts in the largely inaccessible EUV band. These observations provide convincing evidence for a link between the optical/UV blue bump and soft X-ray excess via an extended 'big bump' which peaks in the EUV and which may be comprised of at least two components. Current detectors may soon further resolve this critical band to reveal additional components and the results presented here would then provide a test for the presence of thermal reprocessing structure in the form of dense, Thomson-thin clouds in the innermost central regions of these objects.

## ACKNOWLEDGMENTS

We wish to thank Gary Ferland for his assistance with the workings of his code CLOUDY and the referee, S. Collin-Souffrin, for helpful comments on the manuscript. We are grateful for financial support by the Cambridge Commonwealth Trust (ZK), the Royal Society (AC & MR) and the Italian MURST (AC).

## REFERENCES

- Arnaud K. A. et al., 1985, MNRAS, 217, 105
- Barvainis R., 1993, ApJ, 412, 513
- Bond I. A., Matsuoka M., 1993, MNRAS, 265, 619
- Celotti A., Fabian A. C., Rees M. J., 1992, MNRAS, 255, 419 (CFR92)
- Celotti A., Ghisellini G., Fabian A. C., 1991, MNRAS, 251, 529
- Clavel J. et al., 1992, ApJ, 393, 113
- Collin-Souffrin S., Czerny B., Dumont A.-M., Zycki P. T., 1996, A&A (submitted)
- Courvoisier T. J. L., Clavel J., 1991, A&A, 248, 389
- Czerny B., Elvis M., 1987, ApJ, 321, 305
- de Kool M., Begelman M. C., 1995, ApJ, 455, 448
- Edelson R. A., Malkan M. A., 1986, ApJ, 308, 509
- Elvis M. et al., 1994, ApJS, 95, 1
- Ferland G. J., 1993, Univ. of Kentucky Dept. of Physics and Astronomy Internal Report
- Ferland G. J., Korista K. T., Peterson B. M., 1990, ApJ, 363, L21
- Ferland G. J., Rees M. J., 1988, ApJ, 332, 141 (FR88)
- Field G. B., 1965, ApJ, 142, 431
- Fruscione A., 1995, Proc. IAU Coll. 152 (in press)
- George I. M., Fabian A. C., 1991, MNRAS, 249, 352
- Greveste N., Anders E., 1989, in Waddington C. J., ed, AIP Conf. Proc. 183, Cosmic Abundances of Matter. AIP, New York
- Guilbert P. W., Fabian A. C., McCray R., 1983, ApJ, 266, 466
- Guilbert P. W., Rees M. J., 1988, MNRAS, 233, 475
- Haardt F., Maraschi L., 1993, ApJ, 413, 507
- Johnson W. N., 1994, in Fichtel C. E., Gehrels N., Noms J. P., eds, The Second Compton Symposium. AIP, New York, p. 515
- Kaastra J. S., Roos N., Mewe R., 1995, A&A, 300, 25
- Kolman M., Halpern J. P., Shrader C. R., Filippenko A. V., Fink H. H., Schaeidt S. G., 1993, ApJ, 402, 514

Koratkar A. P., Antonucci R., Goodrich R. W., Bushouse H., Kinney A. L., 1995, *ApJ*, 450, 501

Krolik J. H., McKee C., Tarter C., 1981, *ApJ*, 249, 422

Kuncic Z., 1996, PhD thesis, Univ. Cambridge

Kuncic Z., Blackman E. G., Rees M. J., 1996, *Mon. Not. R. Astron. Soc.* (submitted)

Levich E. V., Sunyaev R. A., 1970, *ApJ*, 7, L69

Lightman A. P., White T. R., 1988, *ApJ*, 335, 57

Maisack M. et al., 1993, *ApJ*, 407, L61

Malkan M. A., Sargent W. L., 1982, *ApJ*, 254, 22

Marshall H. L., Carone T. E., Peterson B. M., 1996, *ApJ* (preprint)

Mathews W. G., Ferland G. J., 1987, *ApJ*, 323, 456

McCrory R., 1979, in Hazard C., Mitton S., eds, *Active Galactic Nuclei*. Cambridge University Press, Cambridge, p. 227

Mushotzky R. F., Done C., Pounds K. A., 1993, *ARA&A*, 31, 717

Nandra K., George I. M., 1994, *MNRAS*, 267, 974

Nandra K., Pounds K. A., 1994, *MNRAS*, 268, 405

Nandra K., Pounds K. A., Stewart G. C., George I. M., Hayashida K., Makino F., Ohashi T., 1991, *MNRAS*, 248, 760

Nandra K., Turner T. J., George I. M., Fabian A. C., Shrader C., Sun W.-H., 1995, *MNRAS*, 273, 85

Netzer H., 1990, in Courvoisier T. J.-L., Mayor M., eds, *Active Galactic Nuclei, Saas-Fee Advanced Course 20*. Springer-Verlag, Heidelberg, p. 67

Neugebauer G., Green R. F., Matthews K., Schmidt M., Soifer B. T., Bennet J., 1987, *ApJS*, 63, 515

Osterbrock D. E., 1985, in Miller J., ed, *Astrophysics of Active Galactic Nuclei and Quasi-Stellar Objects*. University Science Books, Mill Valley, p. 111

Pounds K. A., Nandra K., Stewart G. C., George I. M., Fabian A. C., 1990, *Nat*, 344, 132

Puchnarewicz E. M. et al., 1996, *Mon. Not. R. Astron. Soc.* (submitted)

Rees M. J., 1984, *ARA&A*, 22, 477

Rees M. J., 1987, *MNRAS*, 228, 47p

Sanders D. B., Phinney E. S., Neugebauer G., Soifer B. T., Matthews K., Green R. F., 1989, *ApJ*, 347, 29

Shields G. A., 1978, *Nat*, 272, 706

Shields J. C., Ferland G. J., Peterson B. M., 1995, *ApJ*, 441, 507

Sivron R., Tsuruta S., 1993, *ApJ*, 402, 420

Stern B. E., Poutanen J., Svensson R., Sikora M., Begelman M. C., 1995, *ApJ*, 449, L13

Sun W.-H., Malkan M. A., 1989, *ApJ*, 346, 68

Sunyaev R. A., 1971, *SvA*, 15, 190

Svensson R., Zdziarski A. A., 1995, *ApJ*, 436, 599

Tanaka Y. et al., 1995, *Nat*, 375, 659

Tananbaum H. et al., 1979, *ApJ*, 234, L9

Turner T. J., Pounds K. A., 1989, *MNRAS*, 240, 833

Walter R., Fink H. H., 1993, *AA*, 274, 105

Wilkes B. J., Elvis M., 1987, *ApJ*, 323, 243

Williams O. R. et al., 1992, *ApJ*, 389, 157

Wisotzki L., Dreizler S., Engels D., Fink H. H., Heber U., 1995, *A&A*, 297, L55

Zdziarski A. A., Johnson W. N., Done C., Smith D., McNaron-Brown K., 1995, *ApJ*, 438, L63

Zdziarski A. A., Magdziarz P., 1996, *MNRAS*, 279, L21